Int J Clin Exp Med 2016;9(10):19195-19203
www.ijcem.com /ISSN:1940-5901/IJCEM0027588

Original Article

Susceptibility weighted imaging improved diagnostic accuracy of magnetic resonance in characterization of parotid gland lesions

Wei Zhang[1*], Guan-Qiao Jin[1*], Jun-Jie Liu[2*], Li-Li Wang[3], Dong Xie[1], Ning-Bin Luo[1], Xiang-Yang Huang[1], Dan-Ke Su[1]

Departments of [1]Radiology, [2]Diagnostic Ultrasound, [3]Bone and Tissue-Neurosurgery, Affiliated Tumor Hospital of Guangxi Medical University, Nanning 530021, P. R. China. [*]Equal contributors.

Received March 6, 2016; Accepted June 5, 2016; Epub October 15, 2016; Published October 30, 2016

Abstract: Objective: The purpose of this study was to clarify the diagnostic value of susceptibility weighted imaging (SWI) for distinguishing malignant from benign parotid gland lesions by Magnetic Resonance. Methods: This research prospectively collected the preoperative SWI findings of 41 patients including 12 malignant and 29 benign parotid gland lesions which were confirmed by surgical pathology later. The venous distribution, the maximum diameter of veins ($d_{v\text{-}max}$), the degree of intralesional susceptibility signal (ITSS) and the ITSS per unit area (N/S_{ITSS}) were further analyzed with SPSS 16.0 software. Result: The venous distribution ($P<0.01$), the $d_{v\text{-}max}$ ($P<0.01$), and the ITSS grading ($P<0.01$) of parotid gland lesions were significantly different between malignant and benign lesions, while N/S_{ITSS} ($P=0.367$) was statistically insignificant. When the Youden index reached the highest point, the optimum thresholds of $d_{v\text{-}max}$ was 1.8 mm and ITSS grading was greater or equal to 2. The corresponding areas under the ROC curve (AUC) were 0.924 and 0.856 respectively. Conclusion: The results provided evidence that imaging features of SWI may be helpful in distinguishing malignant from benign parotid gland lesions and worth to be generalized in parotid gland MR scanning.

Keywords: Parotid gland, MR imaging, SWI

Introduction

Preoperative prediction of the benignancy or malignancy of parotid gland lesions is very important for making surgical planning, because an appropriate approach can be chosen to treat lesions accordingly. In addition, when appointing a preoperative diagnosis, it is meaningful to avoid unnecessary surgery in case of benign lesions or consider extensive surgery to remove the entire parotid gland and the surrounding lymph nodes in case of malignant lesions [1-3]. Fine-needle aspiration cytology is usually regarded as a minimally invasive method for the preoperative diagnosis of parotid gland lesions. However, it is not always convincing because sometimes specimens are insufficient due to that some lesions locate too deep to approach or the lesion size is too small to obtain. Moreover, it increases the difficulty of surgical removal of the lesion and the odds of local recurrence [4].

The features of malignancy of the parotid gland include infiltration into surrounding structures and irregular margin on conventional MRI [2], low wash-out in dynamic contrast material-enhanced MRI [5, 6], and the apparent diffusion coefficient (ADC) value less than 1.0×10^{-3} mm^2/sec or greater than 1.4×10^{-3} mm^2/sec on diffusion weighted imaging [3]. It has been shown that high-grade malignant parotid gland lesions usually have ill-defined borders and signal intensity heterogeneity [5, 7]. On the other hand, it has been observed that lesion borders, signal intensity, and heterogeneity were not the factors which correctly differentiate the malignant from benign parotid gland lesions [8]. Infiltration into subcutaneous fat was found not only in malignant parotid gland lesions, but also in those with inflammatory lesions [3]. Our previous study has reported that the wash-out ratio was different between malignant and benign parotid gland lesions using multi-phasic computed tomography (MSCT) [9]. Neverthe-

Table 1. Histopathological diagnoses of parotid gland lesions

Histological findings	Number of lesions
Benign lesions	29
Pleomorphic adenoma	16
Warthin tumour	9
Granulomatous inflammation	2
Tuberculosis	1
Kimura disease	1
Malignant lesions	12
Acinic cell carcinoma	6
Mucosa associated lymphoid tissue lymphoma	2
Squamous cell carcinoma	2
Mucoepidermoid carcinoma	1
Carcinoma ex pleomorphic adenoma	1

less, the wash-out ratio of pleomorphic adenomas was similar to some malignant lesions [9]. Thus, the role of conventional MRI or CT in the distinguish of malignant and benign parotid gland lesions was not very affirmative. The overlap feathures of malignant and benign lesions requires further discrimination for accurate preoperative diagnosis [3, 5, 10-16].

Susceptibility weighted imaging (SWI) is a long-TE fully flow-compensated high-resolution 3D gradient-echo sequence that maximizes the sensitivity to susceptibility effects [17, 18], with filtered-phase information to both create the contrast in magnitude images and add the susceptibility difference between tissues. These characteristics promise SWI to have exquisite sensitivity to the detection of venous deoxyhemoglobin and tumor venous vascularity [17-20]. It provides additional diagnostic information that is usually complementary to conventional MRI sequences to evaluate various neoplasms [17, 19, 20]. Growth of tumor mass is reliant on the proliferation of pathologic vessels, such as gliomas [19]. Microhemorrhages usually occur in aggressive tumors. Thus, tumor vascular hyperplasia and hemorrhage are important in tumor grading [17, 19-22]. In human glioma cells, it has been shown that the levels of ferritin and transferrin receptors are correlated with tumor grade [23]. Previous studies showed that the intratumoral venous vasculature, hemorrhage and the level of transferrin receptor can be detected with SWI [17, 19-22].

However, the value of SWI on the diagnosis of parotid gland lesions has not been studied. In this study, we prospectively assessed the difference of preoperative venous distribution, the maximum diameter of veins ($d_{v\text{-}max}$), the degree of intralesional susceptibility signal (ITSS) and the TISS per unit area (N/S_{ITSS}) of malignant and benign parotid gland lesions using the SWI technique.

Materials and methods

Patients

This study included 41 patients (21 males and 20 females, 13-86 years old, mean age 47.34 years) with lesions of the parotid gland who underwent preoperative MRI and lesion resection in our hospital from May 1, 2013 through October 31, 2014. All cases had met the following criteria: (a) Without any biopsy or interventional therapy or medical treatment performed on parotid gland lesions before the MR imaging scan; (b) The parotid gland lesions were confirmed by histopathological examination of specimens obtained by operation. The findings shown in the SWI sequences were compared with the pathology. All cases signed informed consent forms, and the institutional review board of our hospital group approved the study. **Table 1** presents details of the types of malignant and benign parotid gland lesions identified.

MRI imaging protocol and image evaluation

MR imaging was performed on 1.5 T clinical MR scanner (Magnetom Avanto, Siemens Healthcare, Erlangen, Germany) equipped with 8-channel phased array head and neck coil. A transverse SWI sequence was performed with 49 ms/40 ms (TR/TE), a field of view of 23 cm, a matrix of 256×256, a flip angle of 15°, a number of averages of 1, a 2 mm section thickness, a 0.4 mm intersection gap, phase encoding direction was from R to L. Phase image, minimum intensity projection (MinP), and magnitude image were reconstructed automatically by the system. Pre-saturated slabs were used to saturate contains air structures. Scanning range included neck and parotid gland zone.

Imaging features including the venous distribution, $d_{v\text{-}max}$, ITSS, and N/S_{ITSS}. Small vein shows contiguous low-signal regions on SWI were observed in consensus by two experienced radiologists (Dong Xie., Guanqiao Jin.; 20 and 15 years of experience in reading parotid gland MRI, respectively) after separate assessment.

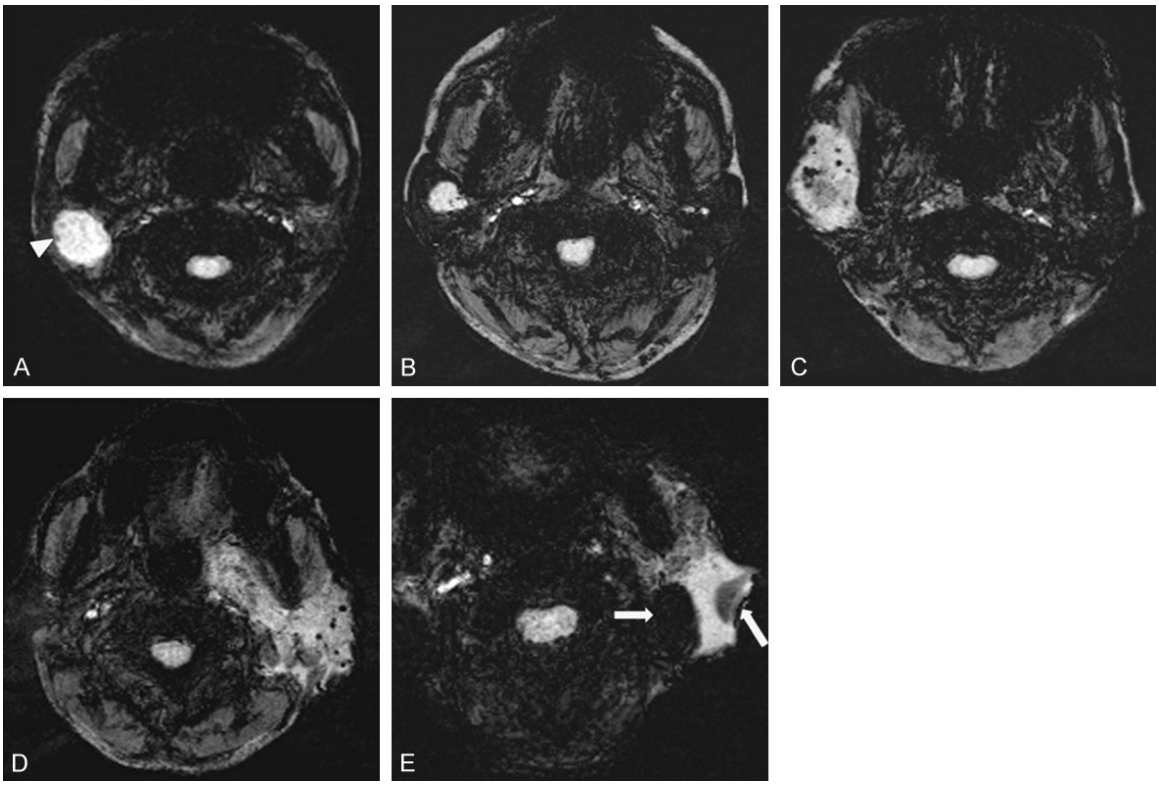

Figure 1. The grade of intralesional susceptibility signals on MinP. A. Is a 27-year-old female with pleomorphic adenoma of the right parotid gland and Grade 0. SWI-MinP shows indistinct fuzzy or inconclusive hypo-intense signals (arrowheads), which was excluded. B. Is a 30-year-old male with Warthin tumour of the right parotid gland and Grade 1. C. Is a 47-year-old female with acinic cell carcinoma of the right parotid gland and Grade 2. D. Is a 57-year-old male with mucosa associated lymphoid tissue lymphoma of the left parotid and gland Grade 3. E. Is a 86-year-old male with acinic cell carcinoma of the left parotid gland and Grade 3. SWI-MinP demonstrates artifacts (arrow).

They obtained the mean measurement of the $d_{v\text{-}max}$ of three times. According to previous findings [24, 25], for semiquantitative analysis, the degree of ITSS was divided into 4 grades on SWI-MinP (**Figure 1**): Grade 0, no ITSS; Grade 1, 1-5 dotlike or fine linear ITSSs; Grade 2, 6-10 dotlike or fine linear ITSSs; and Grade 3, ≥11 dotlike or fine linear ITSSs within a lesion. If a large area of hypo-intense signal within a lesion was defined as Grade 3, it is because artifacts were caused by excessive intralesional hemorrhage or excessive iron deposition (**Figure 1**). N/S_{ITSS} was defined as the ratio, which is the number of hypo-intense signal fine linear or dotlike structures divided by the area of the maximum transverse of lesion.

Histopathologic analysis

An experienced pathologist (Jun Chen, 16 years experience) interpreted and confirmed the pathological diagnosis from hematoxylin-eosin stained specimens and, if necessary, immunehistochemical identification.

Data analysis

Statistical analysis was performed with SPSS version 16.0 software (SPSS, Chicago, Ill). The Chi-square test was used to assess the venous distributions between benign and malignant lesions. The Mann-Whitney U-test was assessed to compare the significance of between-group differences of ITSS grading between malignant and benign lesions. The independent T-test was performed to assess the $d_{v\text{-}max}$, and the N/S_{ITSS} between malignant and benign lesions. Receiver operator characteristic (ROC) curve analysis was used to determine the optimal cut-off value of diagnostic performance of ITSS grading and the $d_{v\text{-}max}$ for malignant lesions. The sensitivity (SE), specificity (SP), positive predictive value (PPV), and negative predictive value (NPV) were calculated from the

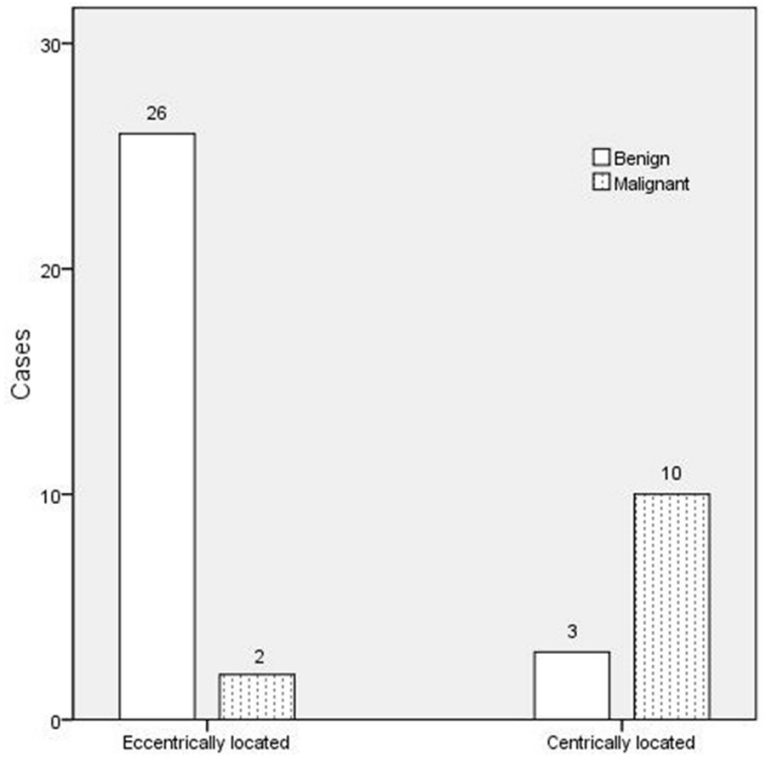

Figure 2. Bar charts of intralesional venous distributions, it shows that eccentrically located in 26/29 (89.7%) and 2/12 (16.7%), centrally in 3/29 (10.3%) and 10/12 (83.3%) of the benign and malignant lesions, respectively.

Table 2. Maximum diameter of intralesional veins of benign and malignant lesions

Parotid gland lesions	Mean (mm)	SD	
Malignant	2.5	1	vs. Benign lesions P<0.01 vs. Pleomorphic adenoma P<0.01 vs. Warthin tumour P<0.01
Benign	1.1	0.5	
Pleomorphic adenoma	1.2	0.5	
Warthin tumour	1.1	0.5	

Note: SD: standard deviation.

ROC curve as the cut-off value used to identify benign and malignant lesions. A *P* value of less than 0.05 was judged as statistically significant.

Results

In 41 lesions (29 benign and 12 malignant), most of intralesional venous distributions were eccentrically located in 26/29 (89.7%) and 2/12 (16.7%) and centrally in 3/29 (10.3%) and 10/12 (83.3%) for the benign and malignant lesions respectively (**Figure 2**). The frequency distribution of veins were significantly more centrally located for malignant than for benign lesions (Chi-square, χ^2=20.882, P<0.01). In the semiquantitative analysis, the Mann-Whitney U-test showed that the differences of ITSS grading were statistically significant between benign and malignant lesions (Z=-3.999, P<0.01). **Table 2** and the independent T-test showed the mean $d_{v\text{-}max}$ of benign lesions was significantly smaller than that of malignant lesions (1.1±0.5 mm vs. 2.5±1.0 mm, t=4.633, P<0.01), whereas the mean N/S_{ITSS} was not significantly different between benign (0.8±0.9 per cm^2) and malignant (1.1±0.7 per cm^2) (t=0.913, P=0.367) (**Figures 3**, **4**). The area under the ROC curve (AUC) of the $d_{v\text{-}max}$ and the degree of ITSS for distinguishing malignant and benign lesions were 0.924 and 0.856, respectively (**Figure 5**). Based on ROC analysis, when the Youden index reached the highest point, the optimum thresholds of $d_{v\text{-}max}$ was 1.8 mm and ITSS grading was greater or equal to 2. In ROC curve analysis, the optimal sensitivity, specificity, PPV, and NPV of venous distributions were 83.3%, 89.7%, 76.9%, and 92.9% respectively; $d_{v\text{-}max}$ were 83.3%, 96.6%, 90.9%, and 93.3% respectively; and ITSS grading were 83.3%, 86.2%, 71.4%, and 92.6% respectively (**Table 3**).

Discussion

SWI is known to be much more sensitive to microhemorrhage, small veins, and blood products (deoxyhemoglobin, methemoglobin, ferritin, and hemosiderin) than other sequences (SE sequences, FSE sequences, FLAIR sequences,

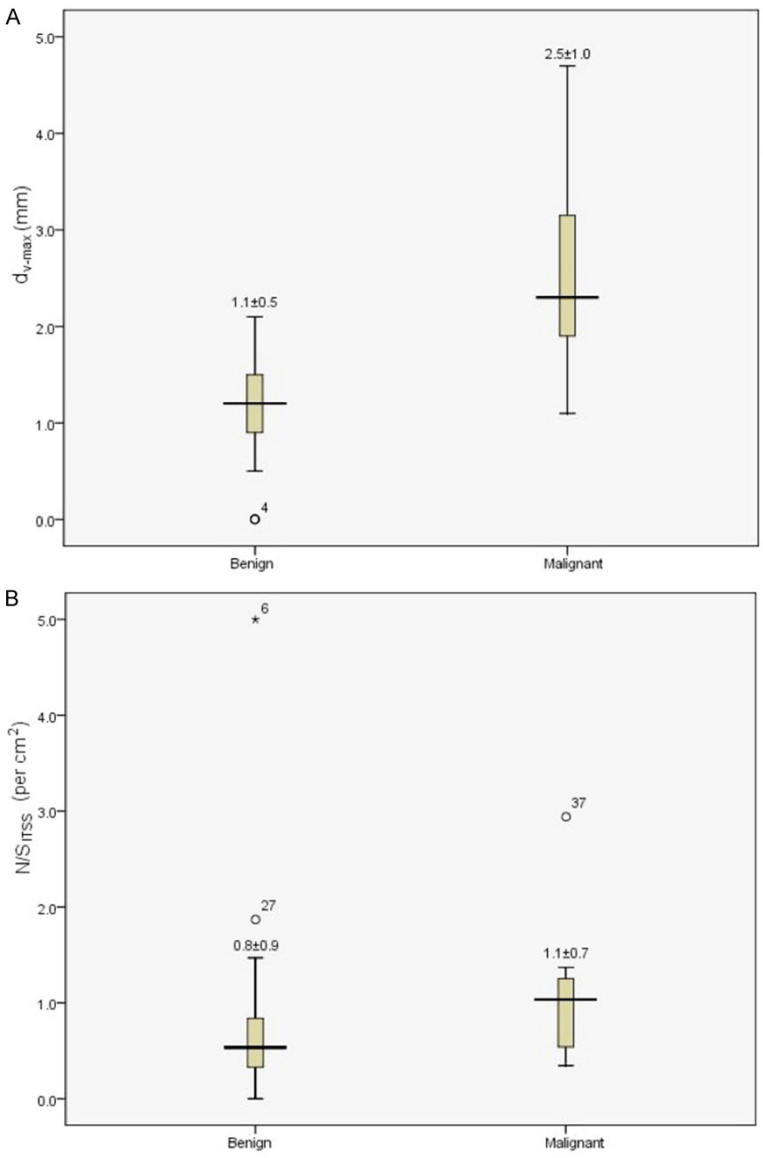

Figure 3. Box plots of (A) $d_{v\text{-}max}$ demonstrates a significant difference (P<0.01) between malignant and benign lesions, while box plots of (B) N/S_{ITSS} was not significantly different (P=0.367). ○ = outlier, * = extreme value.

and GRE sequences). Meanwhile, its high-resolution would enable to detect smaller quantities of small veins and microhemorrhage [17-20]. It makes the identification and quantification of the tumor venous vascularity theoretically possible. Furthermore, it may be possible to avoid performing unnecessary biopsy or surgery for benign lesions and missing malignant lesions in the parotid gland.

From the data that we obtained in the present study, this research concluded that the venous distribution of benign parotid gland lesions mainly manifested the peripheral vascularization, while that of malignant lesions of parotid gland is centrally-located. Simultaneously, a comparison of SWI findings and pathology results shows promising correlations. It is supposed that the course of vascularization and the cell biological behavior formed another focal point in the differentiation. Therefore, we assumed that the central vascularization was more frequent in malignant tumors. In the case of malignant tumors, the growth pattern was usually rapid and aggressive; the vessels were chiefly embedded or even destroyed by tumors and the tortuous or irregular courses of vessels penetrated the tumor. Conversely, benign tumors' growth was slow and expansive, and the vessels were gently curved and randomly along the border of lesions [26-28]. In addition, malignant tumor neoangiogenesis provides neoplastic cells with oxygen and nutrients, which primarily starts in venules infiltration into the neoplastic cells spaces.

The results clearly show that the $d_{v\text{-}max}$ of malignant lesions are statistically significantly wider than that of benign ones, which is consistent with the results of SWI in pathology studies. The widening of vessels caliber for an increase in blood volume meet the demand of the progressive growth of neoplastic cells. On the other hand, malignant tumor neo-angiogenesis is histologically characterized by lack of continuous homogeneous basement membranes, muscular layers, integrated endothelial cells, and extreme nerves [26-29]. The vessel wall has no autonomic function of systole and diastole. The increase of blood flow perfusion will eventually lead to the widening of vessels. Third, this study observed that the vessels of benign lesions were similar in size, while the

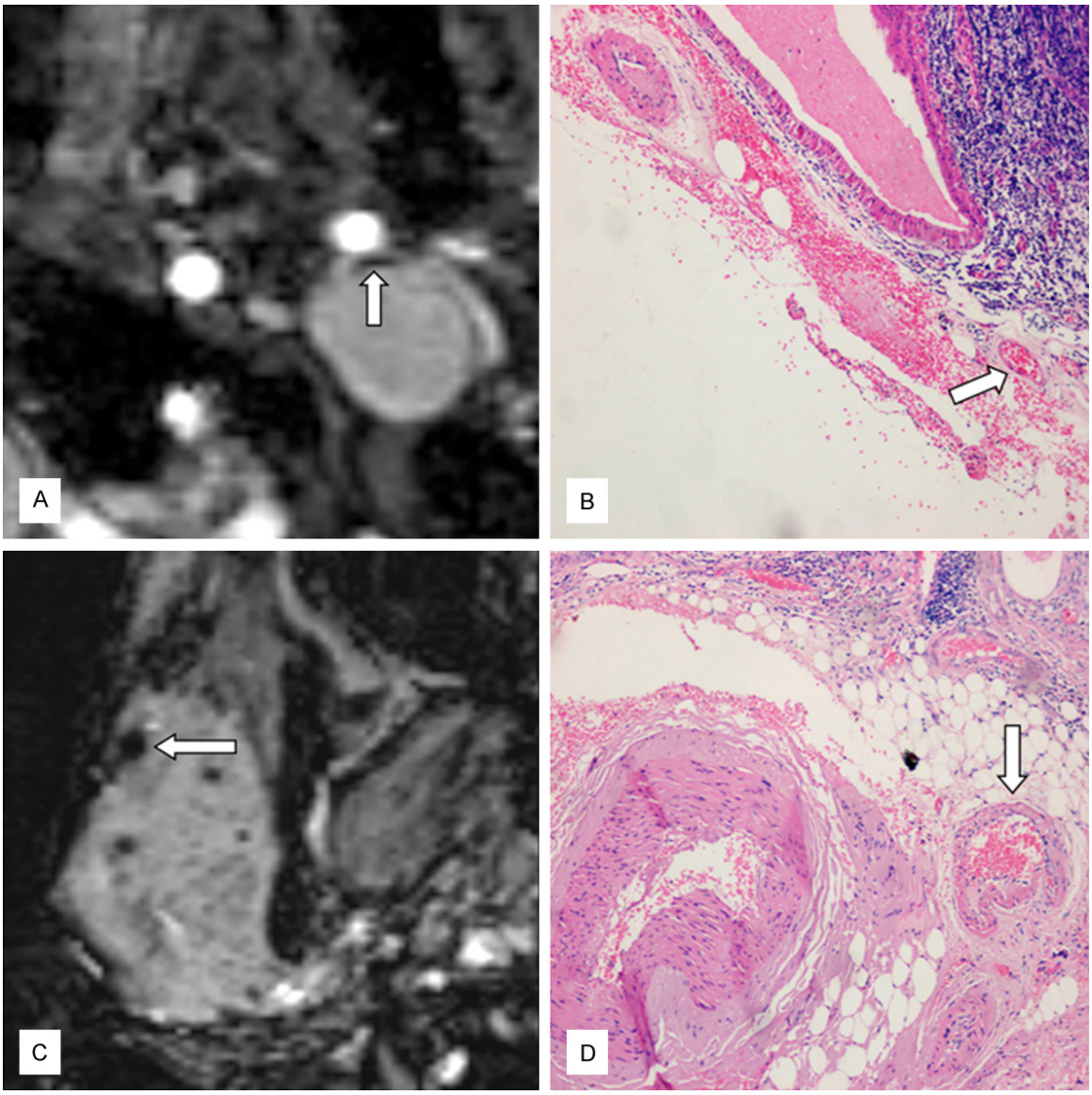

Figure 4. Warthin tumour of the left parotid gland in a 45-year-old man. A: Transverse magnified SWI shows fine-linear ITSS diameter within lesion of approximately 1.1 mm. B: Photomacrograph (haematoxylin-eosin stain, original magnification 100×) showing the vein of the tumour, which corresponds to the dv-max on SWI. C: Acinic cell carcinoma of the right parotid gland in a 47-year-old woman. Transverse magnified SWI shows fine-linear ITSS diameter within lesion of approximately 3.8 mm. D: Photomacrograph (haematoxylin-eosin stain, original magnification 100×) showing the vein of the tumour, which corresponds to the dv-max on SWI.

vessels of malignant lesions were caliber fluctuations, probably because of the presence of arteriovenous shunts and sinusoids. Furthermore, the tumor vessels will be widened with the impact of high-speed blood flow because of the presence of arteriovenous shunts.

According to previous findings [24, 25], ITSS was defined as hypo-intense signal fine linear or dotlike structures, with or without conglomeration, within a lesion was evaluated on SWI-MinP, while excluded indistinct fuzzy or inconclusive hypo-intense signals because the quantification may be subjective and ITSS grades are not accurate. This semiquantitative analysis shows that the differentiation between malignant and benign lesions was statistically significant about the ITSS grade. Malignant lesions had a significantly higher ITSS grade than benign ones. With a low degree of ITSS (grade 0-1), distinguishing between benign and malignant lesions was possible. Furthermore,

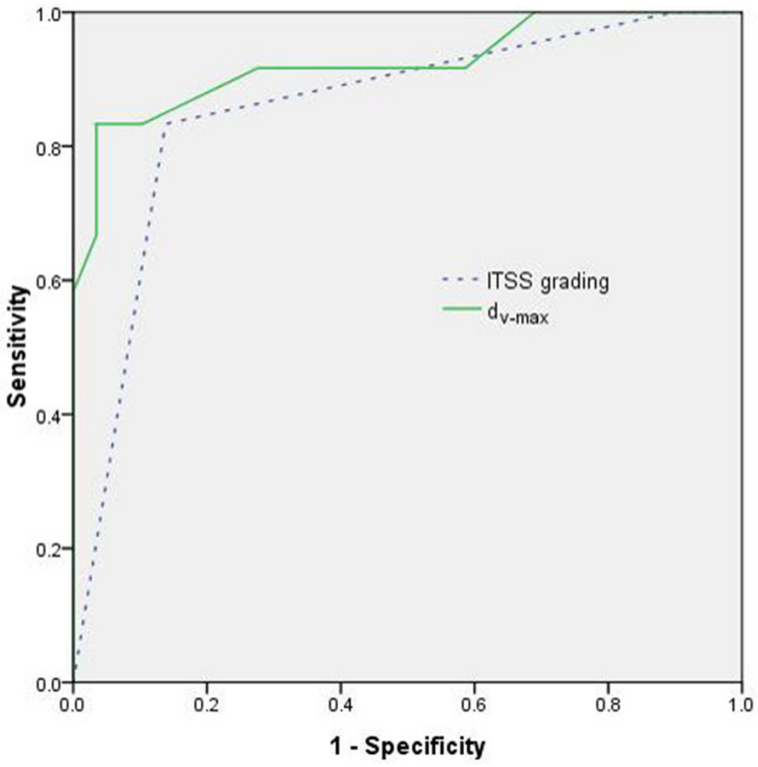

Figure 5. Receiver operating characteristic (ROC) curve of the $d_{v\text{-}max}$ and the ITSS grading used for distinguishing parotid gland lesions from benign to malignant. The Area under cure (AUC) of the $d_{v\text{-}max}$ (solid line) and the ITSS grading (dashed line) are 0.924 and 0.856 respectively.

from the ROC curve analysis, grade 2-3 ITSS provided a specificity of 86.2% (25/29) for differentiating benign and malignant lesions. Thus, further study is warranted to expound the pathophysiologic basis of these differences in the ITSS degree. In the experience, the SWI findings of some benign lesions showed indistinct hypo-intense signals different from ITSSs defined because of rich microvasculature, such as pleomorphic adenoma and inflammatory granulomas. As mentioned above, this result's possible explanation was the vascularization pattern of a multiply. It has been known that the vascular abnormalities architectures of malignant tumors included occlusions, stenoses, loops, and trifurcations occur [27, 30-32]. These would lead to heterogeneous regional flow patterns and blood viscosity heightens. The oxyhemoglobins were over-depleted because of prolonging deprivation of oxygen and production of more deoxyhemoglobins. For another, tumor hypoxic areas usually occur in necrosis.

The studies indicated that despite the fact that intralesional hypo-intense signals were significantly in malignant lesions more than in benign lesions on SWI, the mean N/S_{ITSS} was not statistically significant between malignant and benign. We theorize that the volume of malignant lesions is greater than that of benign lesions from our data.

Our study had some limitations. First, the sample of malignant lesions in the study is relatively small for evaluation of SWI. This study included seven cases of frequently encountered parotid malignancy (mucoepidermoid carcinoma and acinic cell carcinoma). Thus, this study population might reflect the SWI findings. Second, it did not directly reveal that the $d_{v\text{-}max}$ is exactly corresponding with pathology findings, therefore further studies will be necessary. Third, the results show that the $d_{v\text{-}max}$ to be an aid in distinguishing benign and malignant lesions, but this has not been demonstrated in a prospective validity study.

Conclusion

In conclusion, the results provided evidence that imaging features of SWI may be helpful in distinguishing malignant from benign parotid gland lesions, and it is worth to be generalized in parotid gland MR scanning.

Acknowledgements

This study was supported by Guangxi Science and Technology Department research programs (No. 14124004-1-11) and Guangxi Natural Science Foundation Youth Project (No. GXNSFB018089).

Disclosure of conflict of interest

None.

Table 3. Sensitivity, specificity, PPV, and NPV of venous distribution, $d_{v\text{-}max}$, and ITSS degree for distinguishing malignant from benign parotid gland lesions according to threshold values

	SE	SP	PPV	NPV
venous distribution	83.3% (10/12)	89.7% (26/29)	76.9% (10/13)	92.9% (26/28)
$d_{v\text{-}max}$	83.3% (10/12)	96.6% (28/29)	90.9% (10/11)	93.3% (28/30)
ITSS degree	83.3% (10/12)	86.2% (25/29)	71.4% (10/14)	92.6% (25/27)

Address correspondence to: Dan-Ke Su, Department of Radiology, Affiliated Tumor Hospital of Guangxi Medical University, He Di Rd. #71, Nanning 530021, P. R. China. Tel: (86) 0771-5334950; E-mail: sudankegx@163.com

References

[1] Papadogeorgakis N, Skouteris CA, Mylonas AI and Angelopoulos AP. Superficial parotidectomy: technical modifications based on tumour characteristics. J Craniomaxillofac Surg 2004; 32: 350-353.

[2] Sakamoto M, Iikubo M, Kojima I, Sasano T, Mugikura S, Murata T, Watanabe M, Shiga K, Ogawa T and Takahashi S. Diagnostic value of capsule-like rim enhancement on magnetic resonance imaging for distinguishing malignant from benign parotid tumours. Int J Oral Maxillofac Surg 2014; 43: 1035-1041.

[3] Yabuuchi H, Matsuo Y, Kamitani T, Setoguchi T, Okafuji T, Soeda H, Sakai S, Hatakenaka M, Nakashima T, Oda Y and Honda H. Parotid gland tumors: can addition of diffusion-weighted MR imaging to dynamic contrast-enhanced MR imaging improve diagnostic accuracy in characterization? Radiology 2008; 249: 909-916.

[4] Okahara M, Kiyosue H, Hori Y, Matsumoto A, Mori H and Yokoyama S. Parotid tumors: MR imaging with pathological correlation. Eur Radiol 2003; 13 Suppl 4: L25-33.

[5] Eida S, Ohki M, Sumi M, Yamada T and Nakamura T. MR factor analysis: improved technology for the assessment of 2D dynamic structures of benign and malignant salivary gland tumors. J Magn Reson Imaging 2008; 27: 1256-1262.

[6] Witt RL. The significance of the margin in parotid surgery for pleomorphic adenoma. Laryngoscope 2002; 112: 2141-2154.

[7] Christe A, Waldherr C, Hallett R, Zbaeren P and Thoeny H. MR imaging of parotid tumors: typical lesion characteristics in MR imaging improve discrimination between benign and malignant disease. AJNR Am J Neuroradiol 2011; 32: 1202-1207.

[8] Som PM and Biller HF. High-grade malignancies of the parotid gland: identification with MR imaging. Radiology 1989; 173: 823-826.

[9] Jin GQ, Su DK, Xie D, Zhao W, Liu LD and Zhu XN. Distinguishing benign from malignant parotid gland tumours: low-dose multi-phasic CT protocol with 5-minute delay. Eur Radiol 2011; 21: 1692-1698.

[10] Fischer T, Filimonow S, Petersein J, Zimmer C, Beyersdorff D and Guski H. Diagnosis of Heerfordt's syndrome by state-of-the-art ultrasound in combination with parotid biopsy: a case report. Eur Radiol 2002; 12: 134-137.

[11] Freling NJ, Molenaar WM, Vermey A, Mooyaart EL, Panders AK, Annyas AA and Thijn CJ. Malignant parotid tumors: clinical use of MR imaging and histologic correlation. Radiology 1992; 185: 691-696.

[12] Habermann CR, Arndt C, Graessner J, Diestel L, Petersen KU, Reitmeier F, Ussmueller JO, Adam G and Jaehne M. Diffusion-weighted echo-planar MR imaging of primary parotid gland tumors: is a prediction of different histologic subtypes possible? AJNR Am J Neuroradiol 2009; 30: 591-596.

[13] Kato H, Kanematsu M, Watanabe H, Mizuta K and Aoki M. Salivary gland tumors of the parotid gland: CT and MR imaging findings with emphasis on intratumoral cystic components. Neuroradiology 2014; 56: 789-795.

[14] Lechner Goyault J, Riehm S, Neuville A, Gentine A and Veillon F. Interest of diffusion-weighted and gadolinium-enhanced dynamic MR sequences for the diagnosis of parotid gland tumors. J Neuroradiol 2011; 38: 77-89.

[15] Mortele B, Lemmerling M, Seynaeve P, Clarysse P, Quintens F and Kunnen M. Hemangiopericytoma of the parotid gland: CT and MR features. Eur Radiol 2001; 11: 1073-1075.

[16] Yabuuchi H, Fukuya T, Tajima T, Hachitanda Y, Tomita K and Koga M. Salivary gland tumors: diagnostic value of gadolinium-enhanced dynamic MR imaging with histopathologic correlation. Radiology 2003; 226: 345-354.

[17] Li C, Ai B, Li Y, Qi H and Wu L. Susceptibility-weighted imaging in grading brain astrocytomas. Eur J Radiol 2010; 75: e81-85.

[18] Miyake H, Matsumoto A, Hori Y, Takeoka H, Kiyosue H, Hori Y, Mori H, Ueyama S and Kashima K. Warthin's tumor of parotid gland on Tc-99m pertechnetate scintigraphy with lemon juice stimulation: Tc-99m uptake, size,

and pathologic correlation. Eur Radiol 2001; 11: 2472-2478.
[19] Sehgal V, Delproposto Z, Haacke EM, Tong KA, Wycliffe N, Kido DK, Xu Y, Neelavalli J, Haddar D and Reichenbach JR. Clinical applications of neuroimaging with susceptibility-weighted imaging. J Magn Reson Imaging 2005; 22: 439-450.
[20] Sehgal V, Delproposto Z, Haddar D, Haacke EM, Sloan AE, Zamorano LJ, Barger G, Hu J, Xu Y, Prabhakaran KP, Elangovan IR, Neelavalli J and Reichenbach JR. Susceptibility-weighted imaging to visualize blood products and improve tumor contrast in the study of brain masses. J Magn Reson Imaging 2006; 24: 41-51.
[21] Mittal S, Wu Z, Neelavalli J and Haacke EM. Susceptibility-weighted imaging: technical aspects and clinical applications, part 2. AJNR Am J Neuroradiol 2009; 30: 232-252.
[22] Thomas B, Somasundaram S, Thamburaj K, Kesavadas C, Gupta AK, Bodhey NK and Kapilamoorthy TR. Clinical applications of susceptibility weighted MR imaging of the brain - a pictorial review. Neuroradiology 2008; 50: 105-116.
[23] Hammond KE, Lupo JM, Xu D, Metcalf M, Kelley DA, Pelletier D, Chang SM, Mukherjee P, Vigneron DB and Nelson SJ. Development of a robust method for generating 7.0 T multichannel phase images of the brain with application to normal volunteers and patients with neurological diseases. Neuroimage 2008; 39: 1682-1692.
[24] Bagley LJ, Grossman RI, Judy KD, Curtis M, Loevner LA, Polansky M and Detre J. Gliomas: correlation of magnetic susceptibility artifact with histologic grade. Radiology 1997; 202: 511-516.
[25] Park MJ, Kim HS, Jahng GH, Ryu CW, Park SM and Kim SY. Semiquantitative assessment of intratumoral susceptibility signals using non-contrast-enhanced high-field high-resolution susceptibility-weighted imaging in patients with gliomas: comparison with MR perfusion imaging. AJNR Am J Neuroradiol 2009; 30: 1402-1408.
[26] Kallinowski F, Schlenger KH, Runkel S, Kloes M, Stohrer M, Okunieff P and Vaupel P. Blood flow, metabolism, cellular microenvironment, and growth rate of human tumor xenografts. Cancer Res 1989; 49: 3759-3764.
[27] Kim HS, Jahng GH, Ryu CW and Kim SY. Added value and diagnostic performance of intratumoral susceptibility signals in the differential diagnosis of solitary enhancing brain lesions: preliminary study. AJNR Am J Neuroradiol 2009; 30: 1574-1579.
[28] Less JR, Skalak TC, Sevick EM and Jain RK. Microvascular architecture in a mammary carcinoma: branching patterns and vessel dimensions. Cancer Res 1991; 51: 265-273.
[29] Stuhrmann M, Aronius R and Schietzel M. Tumor vascularity of breast lesions: potentials and limits of contrast-enhanced Doppler sonography. AJR Am J Roentgenol 2000; 175: 1585-1589.
[30] Bodner G, Schocke MF, Rachbauer F, Seppi K, Peer S, Fierlinger A, Sununu T and Jaschke WR. Differentiation of malignant and benign musculoskeletal tumors: combined color and power Doppler US and spectral wave analysis. Radiology 2002; 223: 410-416.
[31] Cha S, Knopp EA, Johnson G, Wetzel SG, Litt AW and Zagzag D. Intracranial mass lesions: dynamic contrast-enhanced susceptibility-weighted echo-planar perfusion MR imaging. Radiology 2002; 223: 11-29.
[32] Vaupel P, Kallinowski F and Okunieff P. Blood flow, oxygen and nutrient supply, and metabolic microenvironment of human tumors: a review. Cancer Res 1989; 49: 6449-6465.